The Dielectric Constant at P-Band for Salinity from 0 to 150 PSS

David. M. Le Vine, *Life Fellow, IEEE*, Roger H. Lang, *Life Fellow IEEE*, Ming Li, Emmanuel Dinnat, *Senior Member IEEE*, Jaqueline Boutin, *Member IEEE*, Yiwen Zhou, *Member, IEEE*

***Abstract*—Measurements have been made at P-band (0.707 GHz) to construct a model for the dielectric constant of sea water and extend the model for the dielectric constant to high salinity (50-150 pss). The measurements are part of research to develop a model for the dielectric constant suitable for future wide-bandwidth remote sensing of salinity and for application to water bodies such as the Great Salt Lake with salinity significantly above that found in the open ocean. Measurements have been made at temperatures from 2 to 30 ºC and salinity from 0 to 138 pss. The data have been fit to a Debye model for the dielectric constant with a single resonance as has been employed at L-band (1.413 GHz) where remote sensing of salinity is currently done. Comparison with contemporary models developed from data at L-band indicates that the L-band model and new P-band model do well at both frequencies for salinity less than 50 pss but at higher values of salinity the L-band models diverge from the data. The data has also been used to test at high salinity the mathematical relationship between salinity and conductivity which is the basis for the practical salinity scale (pss).**

***Index Terms*—Dielectric Constant, Sea Water, Microwave, Remote Sensing, Sea Surface Salinity**

I. INTRODUCTION

THE research reported here is part of work to develop a model for the dielectric constant of sea water suitable for future wide-bandwidth remote sensing of salinity. Increasing bandwidth, especially to include frequencies below 1.4 GHz (L-band) where remote sensing of salinity is currently done, is one way to overcome the limitations of reduced sensitivity in cold water [1] [2]. Increased sensitivity will improve remote sensing at high latitudes and near melting ice which are regions of increasing importance in the era of climate change. Models of the dielectric constant of seawater used for remote sensing of salinity [3], [4], [5], [6], [7], [8] are based on measurements at L-band and although they are functions of frequency they have not been tested at lower frequency. In the research reported here, the measurement technique applied successfully at L-band [3], [9] is applied at P-band (0.707 GHz). P-band was selected for the new measurements because it is close to the peak in sensitivity to brightness temperature to salinity [7], [1] and could be done within the context of the existing hardware.

Climate change also impacts inland water bodies such the Great Salt Lake in Utah which have salinity much greater than encountered in the open ocean. Salinity in the southern portion of the Great Salt Lake is typically 145 pss (and even higher in the northern portion) whereas salinity in the global ocean is typically on the order of 34 - 36 pss. Models developed for remote sensing of salinity such as that by Klein and Swift [7] can fail dramatically for salinity out of the range of the measurements on which they were based [10] which is typically salinity below 40 pss. For this reason, it was decided to include high values of salinity in the new measurements.

Measurements have been completed at salinities of 0, 10, 20, 30 ,35, 50, 73, 96, 138 pss and temperatures of 2, 5, 10, 15, 20, 25 and. 30 ºC. The measurements have been made using the resonant cavity approach used successfully at L-band [3], [9]. The L-band measurements were fitted to a Debye model with a single resonance. The same has been done here with the measurements at P-band and a model based on the P-band measurements that includes high values of salinity will be presented (Section III.B). An important question is the frequency dependence of such models (e.g., can a single model with one set of parameters be used over this frequency range). As a check on the frequency dependence, the model based on measurements at P-band will be compared with the model based on measurements at L-band and vice-versa.

This paragraph of the first footnote will contain the date on which you submitted your paper for review, which is populated by IEEE. It is IEEE style to display support information, including sponsor and financial support acknowledgment, here and not in an acknowledgment section at the end of the article. For example, "This work was supported in part by the U.S. Department of Commerce under Grant 123456." The name of the corresponding author appears after the financial information, e.g. *(Corresponding author: Second B. Author).* Here you may also indicate if authors contributed equally or if there are co-first authors.

David M. Le Vine is with the Cryospheric Sciences Laboratory, NASA Goddard Space Flight Center, Greenbelt, MD 20771 USA (e-mail: david.m.levine@nasa.gov).

Roger H. Lang is with the Electrical and Computer Engineering Department, The George Washington University, Washington, DC 20052 USA (e-mail: lang@gwu.edu).

Ming Li is with the Electrical and Computer Engineering Department, The George Washington University, Washington, DC 20052 USA (e-mail: mingli@gwu.edu).

Emmanuel P. Dinnat is with the Cryospheric Sciences Laboratory, NASA Goddard Space Flight Center, Greenbelt, MD 20771 USA, and also with the Center of Excellence in Earth Systems Modeling and Observations, Chapman University, Orange, CA 92866 USA (e-mail: emmanuel.dinnat@nasa.gov).

Jacqueline Boutin is with the Laboratoire d"Oceanographie et du Climat: Experimentations et Approches Numeriques–Institut Pierre Simon Laplace (LOCEAN/IPSL), CNRS, IRD, MNHN, Sorbonne Universite, F-75005 Paris, France (e-mail: jb@locean.ipsl.fr).

Yiwen Zhou is with the Swiss Federal Institute for Forest, Snow and Landscape Research WSL, CH-8903 Birmensdorf, Switzerland (e-mail: yiwen.zhou920@gmail.com).

Color versions of one or more of the figures in this article are available online at http://ieeexplore.ieee.org

Fig. 1. Experimental setup for the measurement of the dielectric constant of seawater at P-band. The system is the same as used at L- band except for the resonant cavity which is larger and resonant at 0.707 GHz.

II. MEASUREMENTS

The measurements at P-band use the same resonant cavity approach that was employed successfully at L-band [3], [9]; And except for the cylindrical cavity, which is twice as large in diameter, the laboratory setup is the same as used at L-band [11], [12].

A. Measurement Method

The laboratory setup is shown in Fig. 1. The system consists of a cylindrical cavity designed for transmission-type measurements at 0.707 GHz enclosed in a temperature-controlled water bath plus plumbing to circulate the water and inject the salt water. The salt water is injected through a narrow quartz tube placed along the axis of the cylinder [9]. For the measurements at P-band, the diameter of the cavity is doubled compared to the diameter at L-band, and while the outer diameter of the quartz tube remains the same at 3 mm, the inner diameter was doubled to 0.2 mm. The cavity's height has been kept the same as the L- band height. Keeping the cavity height and outside diameter of the quartz tube the same, allowed for the reuse of the external glassware from the L-band setup.

The temperature of the seawater is controlled using a circulator (device at left of the water tank). The frequency response of the cavity system is measured using two microwave probes placed in the cavity. The S21 parameter is measured with a network analyzer as the frequency is swept across resonance. This resonant curve is measured with and without saltwater flowing in the tube. The diameter of the inner hole in the tube is small so that perturbation theory can be used to calculate the change in the resonant curve when seawater is introduced. Because the hole is small, the system is under pressure to ensure the flow of the sea water.

Using perturbation theory, the dielectric constant can be determined from the change in the resonant frequency curve with and without seawater present [9], [13]:

$$\varepsilon' - 1 = 2C\,\Delta f / f \quad (1a)$$

$$\varepsilon'' = C\,\Delta(1/Q) \quad (1b)$$

where ε' and ε" are the real and imaginary parts of the dielectric constant of sea water, respectively, and where $\Delta f = fo - f$ is the change in the resonant frequency and $\Delta(1/Q) = 1/Q - 1/Qo$ is the change in the resonant curve (Q is the distance between half-power points). The parameter, C, is a calibration coefficient that is determined by making a measurement with a liquid with a known dielectric constant (methanol in these measurements).

The resonant curve is sampled by the network analyzer at 1600 points over the bandwidth of the sweep. The sweep is repeated 16 times and the results averaged. Two methods are used to determine the f and Q in (1) from this average. One is an algorithm provided by the network analyzer for selecting points representative of the peak and half-power point. The second is to first fit the sample points with a curve. In this method all the points larger than 4 dB down from the peak are selected and fit to a second order polynomial (minimum least square fit). The frequency, f, at the peak and the Q are read from this curve.

This process is repeated with and without salt water in the tube. After each set of measurements, the tube is "washed" with distilled water. The tube is considered clean when the resonant frequency returns to the value for an empty tube at the temperature being used. Each measurement is repeated several times until a consistent set of real and imaginary parts for the dielectric constant are obtained. Three values are averaged to comprise the final result. (See Section 3.2 in [9] for additional details.) The data reported in Tables I-II below were obtained with the curve fitting approach and the three values averaged were those with the smallest standard deviation.

B. Sea Water

The sea water for these experiments was provided by Ocean Science International Ltd (OSIL). For salinity < 40 pss, this is "standard" sea water, and the same water as was used in the measurements at L-band [9]. For salinity in this range, the salinity was measured with an Autosal instrument following standard procedure. This is essentially a conductivity measurement. The instrument measures the ratio of the conductivity of the sample to that of a reference and then, given the temperature, converts the ratio to salinity using equations that have been adopted by international agreement [14], [15]. These equations are the implementation of the definition of the practical salinity scale [16], [14] but they have not been tested above 42 pss. The internationally accepted recommendation for higher salinity is to use dilution [14]. This is what was done by OSIL to provide samples at higher salinity. A sample of standard water was boiled to remove water and increase the salinity to an estimated value of near 150 pss. This water was then diluted with pure water to reach a salinity near 35 pss and

the salinity of the diluted water was measured with a calibrated instrument design to measure salinity in the range, the Autosal. Knowing the original volume and the amount of water added, the original salinity could be determined. This process resulted in salinity samples of 49.6, 73.2, 96.1 and 138.2 pss.

C. Data

Using the equipment shown in Fig. 1 and the procedure described above, measurements were made at temperatures of T = 2, 5, 10, 15, 20, 25, and 30 °C and for salinities of S = 0, 10, 20, 30, 35, 49.5, 73.2, 96.1 and 138.2 pss. The measured values of the real and imaginary part of the dielectric constant are listed in Tables I and II. The first column in each table lists the temperature of the measurement and the first row gives the salinity. The other rows and columns are the measured real part (Table I) and imaginary part (Table II) of the dielectric constant.

Table I: Real Part of the Dielectric Constant: The first column is the temperature (°C) and the first row is the salinity (pss).

	0	9.9930	20.0040	29.9990	34.9940	49.6480	73.2580	96.1500	138.202
2.0000	85.7900	83.5400	81.1600	78.9800	78.2100	76.6700	70.4700	65.5200	57.5800
5.0000	84.8800	82.2800	80.1100	78.3500	76.9300	75.1200	69.2700	64.7000	56.8400
10.0000	82.7100	80.8700	78.8500	76.9400	75.6300	72.1000	67.0000	63.7100	56.9100
15.0000	81.2700	79.2000	77.3600	75.6100	74.0600	71.3900	65.9200	62.9500	54.2300
20.0000	79.1200	77.2700	76.8000	73.8100	73.2100	69.5100	65.2700	61.7300	54.5400
25.0000	77.6900	76.3600	74.1300	72.2600	71.7500	68.3300	64.1800	60.8000	54.1000
30.0000	76.2000	74.9900	72.9400	71.0200	69.2800	66.4600	62.5200	59.5700	52.8100

Table II: Imaginary Part of the Dielectric Constant: The first column is the temperature (°C) and the first row is the salinity (pss).

	0	9.993	20.004	29.999	34.994	49.648	73.258	96.150	138.202
2.000	-5.940	-30.770	-53.050	-73.690	-83.120	-112.260	-156.030	-190.400	-246.590
5.000	-5.360	-32.460	-56.340	-78.400	-89.570	-120.110	-166.550	-205.480	-270.030
10.000	-4.310	-35.090	-61.970	-88.640	-101.310	-135.190	-187.110	-232.770	-305.420
15.000	-3.660	-38.980	-69.580	-98.690	-115.220	-150.840	-206.110	-256.920	-321.190
20.000	-3.100	-42.030	-76.980	-109.300	-124.320	-168.320	-232.960	-290.050	-380.300
25.000	-2.670	-46.280	-84.110	-119.950	-136.410	-184.440	-256.630	-310.380	-420.130
30.000	-2.340	-50.250	-92.050	-131.440	-149.240	-202.870	-281.600	-350.470	-459.970

III. Model Fit

A. Functional Form

The dielectric constant of sea water at the long wavelength end of the microwave spectrum (i.e., below 2 GHz) has the following form [8], [17]:

$$\varepsilon_{sw} = \varepsilon_\infty(S,T) + \frac{\varepsilon_s(S,T) - \varepsilon_\infty(S,T)}{1 + j\omega\tau_{sw}(S,T)} - \frac{j\sigma(S,T)}{\omega\varepsilon_0} \quad (2)$$

The first two terms represent the effect of polarization of the water molecule in the presence of an electromagnetic field as derived by [18]. The last term is the contribution of current which flows when salt is added to pure water. In this expression ω is the radian frequency and σ is the conductivity of the water. Experimental evidence supports this functional form for pure water near L-band with a relaxation time, τ, of about 0.01 ns (corresponding to about 15 GHz). For higher frequencies, the evidence suggests that additional "resonances" are needed [19], [20] and for very high frequencies, a series of resonances has been suggested [21]. However, the next resonance is near 120 GHz, and for applications at L-band (1.4 GHz) and below these higher order terms are not significant.

The problem with fitting (2) to measurements of the dielectric constant is that, except for frequency, ω, and ε_0, all of the parameters are unknown. This includes the first term, ε_∞, the static term, ε_s, the relaxation term, τ, and even the conductivity, σ. To limit the number of unknowns, the following assumptions will be made:

(1). The first term $\varepsilon_\infty = 4.9$: Mathematically this term is the limit when $\omega \rightarrow \infty$. However, the functional form changes as the frequency is increased (e.g., other resonances appear) and (2) no longer applies well before this limit is reached. Conclusive evidence for the value of this parameter does not exist. However, in most models it has a value near 4.9 as originally proposed by [7] although some models include a temperature dependence [6] and even a temperature and salinity dependence [4]. This is essentially a free parameter but obvious the choice effects the fit to other parameters. The assumption $\varepsilon_\infty = 4.9$ made here was also made in the models of [3], [22] which use the L-band data obtained using the same apparatus as employed here.

(2). The relaxation time, $\tau = \tau(0,T)$: The relaxation time for distilled water, $\tau(0,T)$, will be used in the model developed here. This assumption has been used successfully in building models at L-band [3], [4], [5], [6], [7], and one can argue that the relaxation time should be at most weakly dependent on salinity [17]. Hence the assumption will be made that:

$$\tau(S,T) = \tau(0,T) \quad (3a)$$

(3). Static term, $\varepsilon_s(S,T)$: In the case of zero salinity, the first two terms on the right in (2) are the dielectric constant of pure water. Hence, in the general case when $S \neq 0$ the static term, $\varepsilon_s(S,T)$ can be written in the form [17]:

$$\varepsilon_s(S,T) = \varepsilon s(0,T)\,[1 + S\,R(S,T)] \quad (3b)$$

where $\varepsilon_s(0,T)$ is the static term in the case of pure water and $R(S,T)$ is a function to be determined. Both $\varepsilon_s(0,T)$ and $R(S,T)$ are to be determined by fitting the model to the data. In the fitting to follow polynomials in T or S and T as appropriate will be used for these functions.

(4). Conductivity, $\sigma(S,T)$: Most contemporary models used in remote sensing of salinity use an expression for conductivity inverted the definition of the practical salinity in terms of

conductivity and temperature [16] to form a relationship giving conductivity as a function of salinity and temperature. This relationship was improved at low salinity and formally adopted by the international community [14]. However, the measurements which established this definition only cover salinity up to 42 pss. One of the goals of the research presented here is to build a model for the dielectric constant that will apply to water bodies with much higher salinity. Consequently, this expression will not be used here, and conductivity will be treated as parameter to be determined by the measurements. A polynomial in S and T will be used to model σ(S,T) similar to the approach employed by [9] and [3] at L-band but in their case the data was limited to S < 38 pss. As a check on the fit, one would expect the expression derived for σ(S,T) from the new P-band data to be close to that in [14] for S < 40 pss. Assuming this the case, then the values of σ(S,T) at higher salinity can be used to check the validity of the conventional expression in [14] at salinity larger than 42 pss.

B. Fitting Model to Data

1) Distilled water

The first step in fitting the model in Eqn 1 to the data is to determine the unknown parameters for distilled water: the relaxation time, $\tau(0,T)$ and the static term, $\varepsilon_s(0,T)$. The procedure adopted here is the same as outlined in [3]. Setting $\sigma = 0$ in (2) and S = 0 in (3b) and with a little bit of rearranging, one can solve for the relaxation time in terms of the measured values of the real part and imaginary part of the dielectric constant. The result is given in (4a). Then using this expression for $\tau(0,T)$ one can solve for the static term, $\varepsilon_s(0,T)$. This result is given in (4b):

$$\tau(0,T) = \varepsilon'' / (\omega \varepsilon' - \varepsilon_\infty) \quad (4a)$$

$$\varepsilon_s(0,T) = (\varepsilon' - \varepsilon_\infty)(1 + (\omega \tau(0,T))^2 + \varepsilon_\infty \quad (4b)$$

A third order polynomial in T was selected to represent $\tau(0,T)$ and $\varepsilon_s(0,T)$. The Matlab routine, "polyval", was used to determine the coefficients of the polynomial. An independent fit was also made using an MLS solution (pseudo inverse) with little difference. In the first step a fit was made for $\tau(0,T)$. An additional set of measurements at 35 °C that did not include the high values of salinity but did include S = 0 was included only for purposes of this fit. Then the resulting polynomial model for $\tau(0,T)$ was used in (4b) with the measured real part of the dielectric constant for distilled water to obtain a fit for the polynomial representing $\varepsilon_s(0,T)$. The results are:

$$\tau(0,T) = [\, 1.7953869 + 0.0695501\, T - 0.0017650\, T^2 + 0.0000205\, T^3 \,]\, 10^{-11} \quad (5a)$$

$$\varepsilon_s(0,T) = 87.0887057 - 0.4000733\, T + 0.00000083\, T^2 + 0.00004251\, T^3 \quad (5b)$$

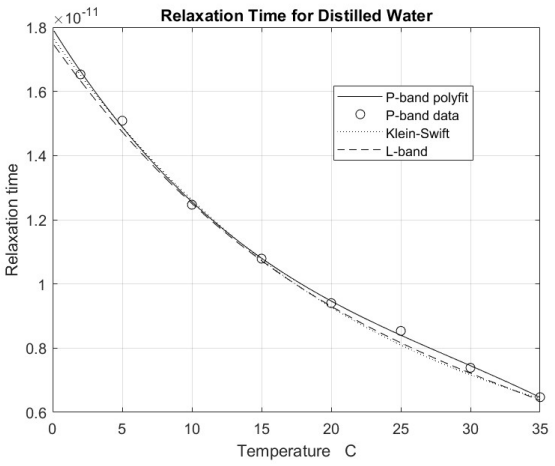

Fig. 2. The relaxation time for distilled water. The solid black line is the fit to the P-band data and the symbols, "o", are the data. The dashed line is the result from the L-band measurements [3] and the dotted line is the result reported by [7].

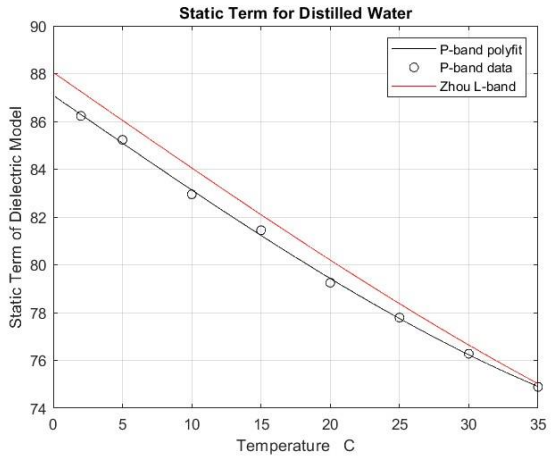

Fig 3: Static term for distilled water. The solid black curve is the model and the symbols, "o", are the data. The solid red curve is the static term at L-band from [3].

The models for $\tau(0,T)$ and $\varepsilon_s(0,T)$ are shown in Figs 2-3. The solid curve in Fig. 2 shows the relaxation time, $\tau(0,T)$, given in (5a) as a function of temperature. For comparison, the relaxation time for distilled water obtained using a similar procedure applied to the measurements at L-band [3] is given by the dashed curve. In addition, the relaxation time reported by [7] and taken from the literature of independent measurements of distilled water is shown with the dotted curve. The symbols, "o", represent the P-band data: the values of $\tau(0,T)$ obtained from (4a) using the measured values of

dielectric constant. The good agreement of the three curves confirms that there is very little variation of the relaxation time with frequency over this relatively narrow frequency range and is a rough check on the quality of the P-band measurements.

Figure 3 shows the static term for distilled water, $\varepsilon_s(0,T)$, obtained with the P-band data (5b). The black curve is the model given in (5b) and the symbols, "o" are the values obtained from (4b) using the measured values of the dielectric constant. Also plotted for reference (red curve) is the static term obtained with the L-band data by [3].

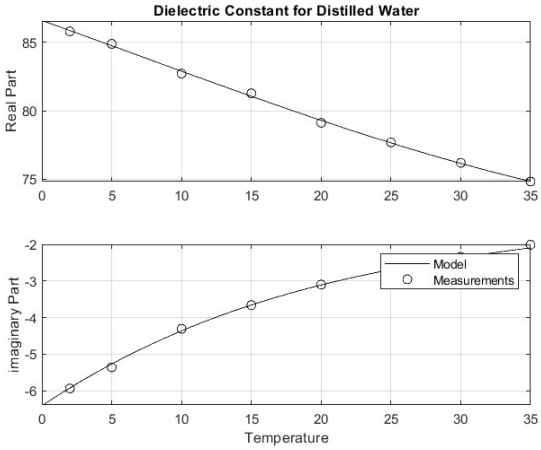

Fig 4: Comparison of model with measurements for distilled water. The solid line represents the prediction of the model and the symbol "o" indicated the measured value. Real part on the top and imaginary part on the bottom.

Figure 4 shows the model of the dielectric constant for distilled water obtained with these parameters (i.e., (1) with $\sigma = 0$ and the parameters $\tau(0,T)$ and $\varepsilon_s(0,T)$ given by (5a) and (5b)) together with the measured values of the dielectric constant. The top panel is the real part and the bottom panel is the imaginary part. The solid line is the value predicted by the model and the symbols are the measured values.

2) General Case: Model with Salinity

In the general case of salty water it is necessary to include an additional parameter, the conductivity, $\sigma(S,T)$, and to allow for a dependence of the static term on salinity (3b). To accommodate the additional number of unknowns, it has been assumed ((3a)) that the relaxation time is independent of salinity, and the value for distilled water given in (5a) will be used. With this assumptions and following the same procedure as for the case of distilled water and described by [3], the real and imaginary parts of (1) can be rearranged to obtain solutions for the unknown functions, $\sigma(S,T)$ and $R(S,T)$:

$$R(S,T) = ((\varepsilon' - \varepsilon_\infty) (1 + (\omega \tau)^2) + \varepsilon_\infty) / \varepsilon_s \quad (6a)$$

$$\sigma(S,T) = -(\omega \varepsilon_o)(\varepsilon'' + (\omega \tau) \varepsilon_s - \varepsilon_\infty) / (1 + (\omega \tau)^2) \quad (6b)$$

where ε' and ε'' are the real and imaginary part of the measured dielectric constant, respectively, and ε_s and τ are the values for distilled water.

Adopting the reasoning in [3] the following polynomials are assumed for the unknown functions, $\sigma(S,T)$ and $R(S,T)$:

$$\sigma(S,T) = S (q_o + q_1 T + q_2 S + q_3 ST + q_4 ST^2) \quad (7a)$$

$$R(S,T) = p_0 + p_1 T + p_2 S + p_3 ST + p_4 S^2 \quad (7b)$$

The final step is to solve for the unknown coefficients, [p] and [q]. This has been done by equating (6) and (7) using the measured values of ε' and ε'' and the corresponding values of S and T. The result is a linear matrix equation for the unknown [p] or [q] in the form A P = B where A is a 5 x N matrix where N is the number of measurements and P is a 1 x5 matrix of the coefficients, [p]. This equation has been solved for the [p] using the Matlab function, "pinv" (which is equivalent to an MLS solution). The results are:

P = (242.8975 -0.3911 0.2289 -0.0020 -0.0018)E-5 (8a)

Q = (873.5271 290.6078 -15.1077 -0.9691 0.0136)E-5 (8b)

Figures 5 and 6 show a comparison of the model (i.e., (2) with parameters given by (3), (5), (7) and (8)) with the measurements. Figure 5 reports the comparison of the model predictions (solid lines) and the measured values of the dielectric constant (symbols) as function of salinity for several of the values of temperature included in the measurements. The top panel is the comparison for the real part of the dielectric constant and the bottom panel is the comparison of the imaginary part. Figure 6 presents the comparison as a function of temperature for several values of salinity. As in Fig. 5 the solid lines are the predictions of the model and the symbols are the measurements. The real part is on the top and the imaginary part is on the bottom.

Two metrics have been computed to give an idea of the quality of the fit. These are the root mean square difference (RMSD) between the data and model at the data points and the mean absolute percentage error (MAPE) at these points. As the name implies, the MAPE is the average of the absolute value of the difference between model and measurement expressed as a percentage of the measured value. (See (A.2) in [3] for a mathematical definition of the MAPE.) It is helpful for handling differences which cover a very large range of values such as occurs with the imaginary part.

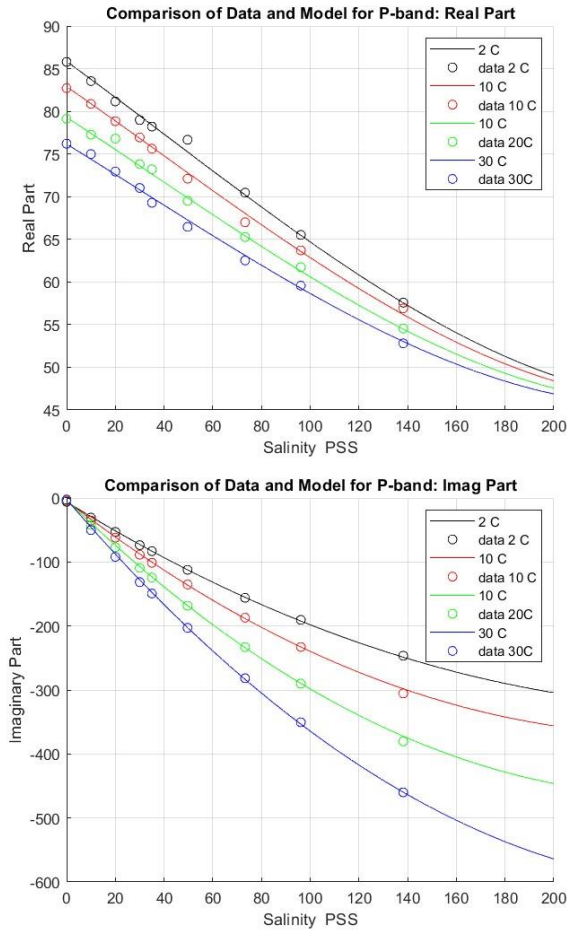

Fig 5: Comparison of model prediction (solid line) with measurements (symbol) at P-band. Real part (top) and Imaginary part (bottom). The comparison is as a function of salinity for a representative selection of values of temperature used in the measurements.

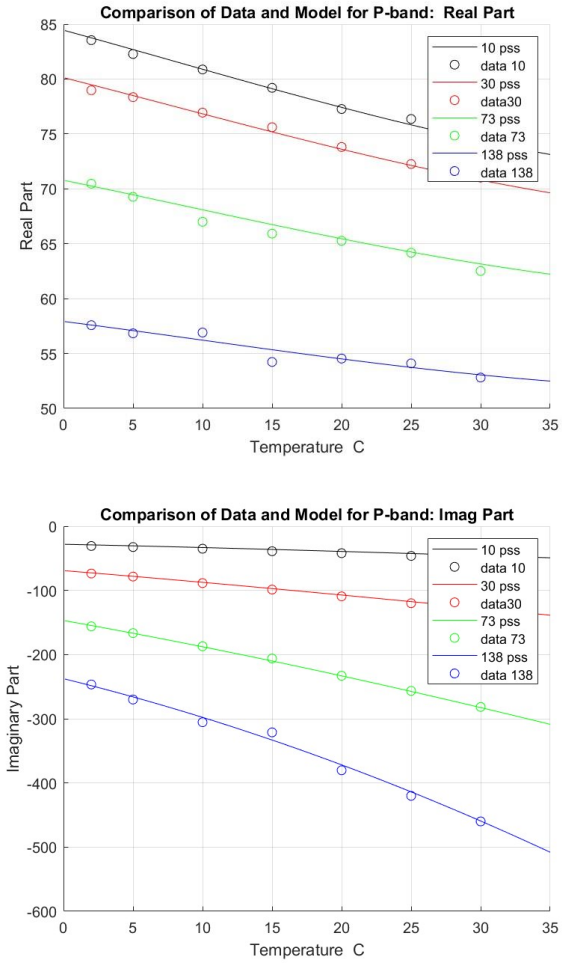

Fig 6. Comparison of model prediction (solid line) with measurements (symbol) at P-band. Real part (top) and imaginary part (bottom). The comparison is as a function of temperature for several values of salinity representative of those used in the measurements.

The MAPE for the real part is 0.51% and 2.0% for the imaginary part, and the RMSD are 3.2 and 0.47 for the real part and imaginary part respectively. These values are larger than those reported for the fit to the L-band data [3] but the L-band data covered a smaller dynamic range ($0 < S < 40$ pss) compared to ($0 < S < 150$ pss) for the P-band measurements and the L-band data included more measurements especially a low temperature. One feature that the statistics for the two models have in common is that the metrics, RMSD and MAPE, for the real part are smaller than those for the imaginary part. The dynamic range of the imaginary part is larger than that of the real part in both data sets which may be part of the reason. Another metric, the RMSD expressed as a percentage of the measured values, has values comparable to the MAPE in the P-band data. These statistics appear to be relatively uniform with respect to temperature and salinity (i.e., about the same at low temperature as at high temperature and about the same at low salinity as at high salinity).

IV. DISCUISSION

A. Frequency Dependence

Understanding the frequency dependence of the model given in (2) is particularly important for future wide bandwidth remote sensing of ocean salinity. The functional form of the model is based on sound physics: it is consistent with Maxwell's equations for bulk media and is based on a reasonable model for the behavior of a water molecule in the presence of an electromagnetic field [17], [18]. It has proven successful for remote sensing of salinity at L-band [23], [24], [25] and, although there is reason to believe it is not complete at high frequencies [20], [8], [4], it should be reasonable for lower frequencies such as P-band. The frequency range in recent proposals for wide bandwidth instruments with application to this portion of the spectrum is about $0.5 < f < 2.0$ GHz [26], [27]. An important question is whether a single

model (i.e., (2) with one choice of parameters) can cover such a frequency range.

To obtain insight regarding this question, the model derived here from the P-band measurements has been compared with the model developed using the same method from the L-band measurements. If the frequency dependence given by the functional form in (2) is valid, then it should not mater at what frequency the measurements are made and the unknown parameters determined from the data. The parameters determined from each set of measurements may be different, but a model based on measurements at P-band should be valid at L-band and vice-versa. Both models should give the same dielectric constant whether evaluated at P-band or at L-band.

This is checked in Figs. 7 and 8. A comparison of the two models both evaluated at L-band is given in Fig. 7 and a comparison of the two models with both evaluated at P-band is given in Fig. 8. The comparison is given as function of temperature on the top and as a function of salinity on the bottom. In each of these figures the red line represents the model derived from the P-band data and the black curves are the predictions of the model based on the L-band data. The dotted, dashed and solid lines are for S = 10, 20, 30 pss, respectively (top panel) and T = 10, 20, 30 ºC, respectively (bottom panel).

In these figures the range of salinity has been limited to 0 < S < 40 pss because this is the range available in the L-band data. The L-band model used in this comparison is that developed by [3] which is based on the complete set of the L-band measurements produced by the team at the George Washington University [3], [9]. It was chosen for comparison because it

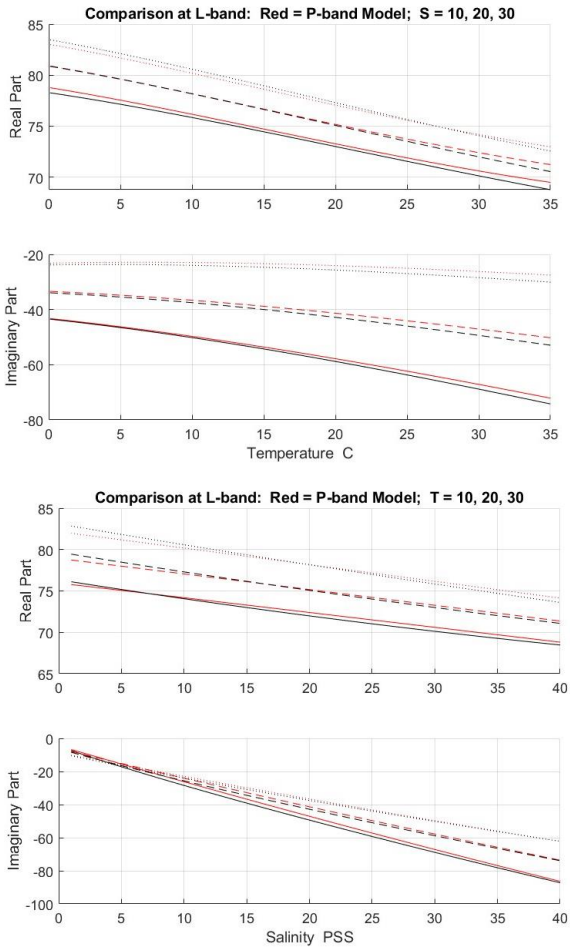

Fig. 7: The comparison of the two models at P-band as a function of temperature for several values of salinity (top) and as a function of salinity for several values of temperature (bottom). The red curves are the P-band model and the black curves are the L-band model. In the top panel the dotted, dashed and solid curves are for S = 10, 20 and 30 pss, respectively. In bottom panel the dotted, dashed and solid curves are for T = 10, 20 and 30 ºC,

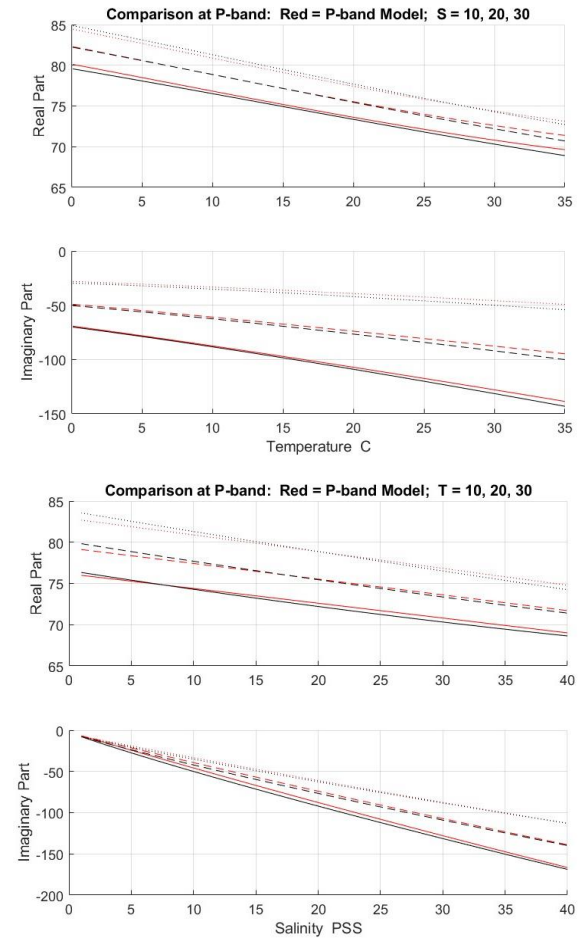

Fig. 8: The comparison of the two models at P-band as a function of temperature for several values of salinity (top) and as a function of salinity for several values of temperature (bottom). The red curves are the P-band model and the black curves are the L-band model. In the top panel the dotted, dashed and solid curves are for S = 10, 20 and 30 pss, respectively. In the bottom panel, the dotted, dashed and solid curves are for T = 10, 20 and 30 ºC,

treats the conductivity, σ(S,T), as an unknown (polynomial) as done here with the P-band data. The P-band model (red) is that developed here based on the full range of salinity (i.e., including high values).

Although the two models are in good agreement whether evaluated at L-band (Fig. 7) or P-band (Fig. 8), there are small differences (e.g., particularly noticeable at high temperatures). However, the RMSD between the two models over this range of temperature and salinity is less than the RMSD between the P-band model and the data used to derive the model. The RMSD for the real part is the same whether the models are evaluated at P-band or L-band and although not identical in the case of the imaginary part, they are reasonably close.

B. High Salinity

The model of [3] fails at high salinity [10]. This is not a surprise because the data used to develop the model did not include values of salinity above 40 pss. An attempt to fix this problem was made by [22] by replacing the term for conductivity in [3] with the expression derived from the definition of practical salinity (i.e., the relationship for σ(S,T) given in the "Thermodynamic Equations of Seawater" [14]) and then refitting to the data. This removed the obvious problems but there was no way to validate the behavior at high salinity because the model was still based on data with S < 40 pss.

The new data at P-band provides a chance to test this change. The examples in Figs. 7-8 and theory suggest that the model in (2) should be valid, at least to first order, at both P-band and L-band and regardless of the value of salinity. Hence, the modifications made by [22] to the model based on the L-band data should also be valid at P-band at all values of salinity. This is true for S < 40. Replacing the model in [3] with the model in [22] in Figs. 7-8 produces no noticeable change. The two models are indistinguishable over this range of salinity. If the change was successful in applying to high salinity also, then the model should also compare well with the P-band model when the range of salinity is extended to higher values.

This comparison is shown in Fig. 9 which shows the two models as a function of salinity for values of salinity up to 200 pss and for T = 10, 20 and 30 ºC. The red curves are the P-band model and the black curves the modified L-band model. The values of temperature are within the range of the measurements used to fit both models. However, the range of salinity 0 < S < 200 includes values which are out of the range of the measurements (S < 40 pss) used to produce the L-band model. That this is a problem is evident whether the models are compared at L-band (bottom figure) or at P-band (top figure). The difference is most evident in the real part (top panels) where it is clear that the two models diverge starting at about S = 70 pss. Since, only the P-band model is based on data in this regime, the difference is an indication of a problem in the L-band model.

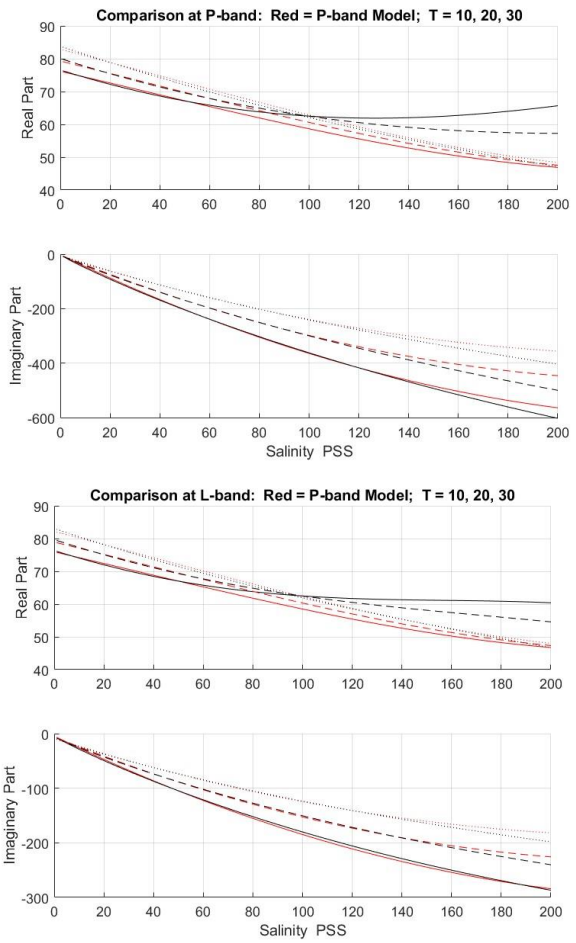

Fig. 9: The fit for all salinity plotted as a function of salinity for several values of temperature. The red curves are the P-band model, and the black curves are the L-band model. The dotted, dashed and solid curves are for T = 10, 20 and 30 ºC, respectively. In the top panel both models are evaluated at P-band (0.707 GHz). In the bottom panel both models are evaluated at L-band (1.413 GHz).

The biggest difference is in the real part (top panel in each figure). Since the conductivity does not contribute to the real part and ε_∞ is real, the problem is an issue with the polynomials used to model the salinity and temperature dependence of the static term, ε_s, and relaxation coefficient, τ, in the L-band model which are only constrained to fit within the range of the data (i.e., S < 40 pss). An example is given the Appendix of another recent L-band model which makes a different choice for these polynomials (essentially R(S,T) in (3b)) with a good fit for S < 40 pss but very different but also poor results at high salinity. To fix this problem, data is needed at high salinity at L-band.

C. Implications to the Model for Conductivity

A difference in the imaginary parts of the two models can also be seen in Fig 9 beginning at about S = 140 pss although this is dependent on temperature. The difference is a little more

pronounced in the comparison at P-band (top). At these values of salinity, the imaginary part is dominated by the last term in (2) which suggests that the expression for σ(S,T) is the source of the discrepancy.

The L-band model used in these figures [22] uses the expression for σ(S,T) given in the "Thermodynamic Equations of Seawater" [14]). This expression is based on the definition of practical salinity, but it has only been validated for S < 40 pss [14], [15]. The expression for σ(S,T) from [14] is compared with the model derived from the P-band data in Fig. 10. The plot reports the two expressions for conductivity for several values of salinity over a range of temperature for which both models are valid. In the case, S < 40, for which both models are also valid, the two sets of curves are close. However, at high values of salinity (S > 100) a bias between the two models is evident. This bias increases with increasing salinity. But there are also some small differences at low values of salinity, and more work is needed to determine if the difference at high salinity is significant and an indication of an error in the expression for σ(S,T) from [14] at high salinity.

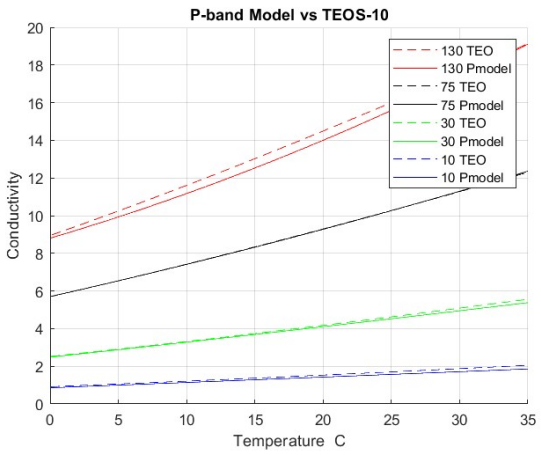

Fig 10: Comparison of P-band model for conductivity, σ(s,T), with [14]. The comparison is given as a function of temperature for several values of salinity. The solid lines are σ from the P-band model and the dashed lines are from [14].

V. CONCLUSION

At values of salinity commonly encountered in the global oceans and lakes (0 < S < 40 pss) the model based on L-band data [3] and the model derived here based on the new measurements at P-band are comparable and apply equally well at either frequency. This is encouraging and supports the use of either model for future wideband remote sensing. On the other hand, small differences are apparent, and more work is needed to determine if a model which is based on a combination of the L-band and P-band data would be better suited for future wide bandwidth remote sensing.

Significant differences appear at high values of salinity. In part this is because the polynomials used for the parameters (e.g., the static term and conductivity) are not valid representations outside of the range of data used to define them. One possible improvement is to use the expression for σ(S,T) based on the definition of practical salinity [15]. This is employed in several contemporary models [8], [6], [4]. However, the examples in Fig. 9 and 11 show that this is only part of the problem and that data including high salinity is needed to get the correct fit for the real part.

The measurement made here provide a chance to test the expression for σ(S,T) given in [15] at high values of salinity. Comparing with the P-band measurements at high salinity (e.g., Fig 9, 10) suggest that it is a good approximation but there is evidence that this expression may not extrapolate accurately for salinity greater than about 100 pss.

APPENDIX

Figure 11 illustrates the issue at high salinity with the model reported by [6]. This model uses the form in (2) with σ(S,T) given by the expression in [14] and with τ and ε_∞ the same as used in the model by [5]. The expression for the static term, ε_s. has the form given in (3b) with R(S,T) a polynomial chosen to fit the L-band data and give a best match to the SMOS satellite data.

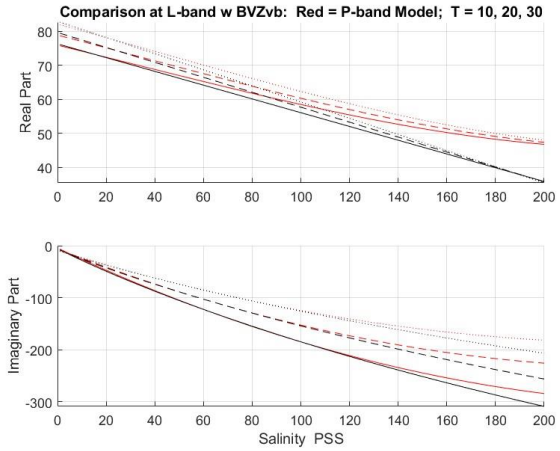

Fig. 11. Comparison at L-band of the model from [6] (black) and the P-band model (red) as a function of salinity for T = 10°C (dotted), 20°C (dashed) and 30°C(solid).

In Fig. 11 the P-band model is given by the red curve and the model of [6] is represented by the black curve. Both models are evaluated at L-band and plotted a function of salinity for several values of temperature. The agreement of the imaginary part

(lower panel) is about same as the agreement of the imaginary parts in Fig. 8 where a similar comparison is made using the model of [22]. The similar behavior is because both models use the same expression (i.e., from [14] for the conductivity, σ(S,T)), and the conductivity term dominates the imaginary part at high salinity. But the behavior is not similar in the case of the real part. As in Fig. 8, the real part agrees with the P-band model for low salinity but diverges for salinity above about 100 pss. The form of the divergence from the P-band model is different in Figs 8 and 11. This illustrates that there are many choices for the unknown parameters that will fit the data, but also many ways for these fits to diverge outside of the range of data used to define them. The way to fix this problem is to extend the range of the measurements.

The ideal solution for improving the behavior of the L-band at high salinity is to obtain new measurements at L-band at high salinity and then make a proper fit that includes the values at high salinity. An option is to use the P-band model for cases which involve high salinity (e.g., remote sensing with current sensors at L-band over water bodies such as the Great Salt Lake). Another option is to combine the data sets and define a hybrid model to be used over the entire frequency range between L-band and P-band. This is the subject of on-going work.

REFERENCES

[1] D.M. Le Vine and E. P. Dinnat, “The multifrequency future for remote sensing of sea surface salinity from space,” Remote Sens., vol. 12, no. 9, p. 1381, Apr. 2020, doi: 10.3390/rs12091381.

[2] N. Vinogradova et al., “Satellite salinity observing system: Recent discoveries and the way forward,” Frontiers Mar. Sci., vol. 6, 2019, Art. no. 243, doi: 10.3389/fmars.2019.00243.

[3] Y. Zhou, R.H. Lang, E.P. Dinnat and D.M. Le Vine, “Seawater Debye Model Function at L-Band and Its impact on Salinity Retrieval from Aquarius”, IEEE Trans. Geoscience and Remote Sensing, Vol 59, No 10, October 2021, doi: 10.1109/TGRS.2020.3045771.

[4] T. Meissner and F. J. Wentz, “The complex dielectric constant of pure and sea water from microwave satellite observations,” IEEE Trans. Geosci. Remote Sens., vol. 42, no. 9, pp. 1836–1849, Sep. 2004.

[5] T. Meissner and F. J. Wentz, “The emissivity of the ocean surface between 6 and 90 GHz over a large range of wind speeds and earth incidence angles,” IEEE Trans. Geosci. Remote Sens., vol. 50, no. 8, pp. 3004–3026, Aug. 2012.

[6] J. Boutin et al., "New Seawater Dielectric Constant Parametrization and Application to SMOS Retrieved Salinity," in IEEE Transactions on Geoscience and Remote Sensing, vol. 61, pp. 1-13, 2023, Art no. 2000813, doi: 10.1109/TGRS.2023.3257923.

[7] L. Klein and C. T. Swift, “An improved model for the dielectric constant of sea water at microwave frequencies,” IEEE Trans. Antennas Propag., vol. AP-25, no. 1, pp. 104–111, Jan. 1977.

[8] D.M. Le Vine, R.H. Lang, Y. Zhou, E.P. Dinnat, and T. Meissner, “Status of the Dielectric Constant of Sea Water at L-Band for Remote Sensing of Salinity”, IEEE Trans. Geosci. And Remote Sensing, vol. 60, pp. 1-14, 2022, Art no. 4210114, doi: 10.1109/TGRS.2022.3207944.

[9] R.H. Lang, Y. Zhou, C. Utku, D. Le Vine, “Accurate measurements of the dielectric constant of seawater at L band”, Radio Sci., 51, 2–24, 2016 doi:10.1002/2015RS005776.

[10] D. Le Vine, R. Lang, E. Dinnat, Y. Soldo, P. de Matthaeis, and Y. Zhou, “Dielectric constant model function at extreme salinity,” in Proc. Ocean Salinity Sci. Team Workshop, Apr. 2020, pp. 1–15. [Online]. Available: https://salinity.oceansciences.org/meetings-documents.htm?id=scposst2020.

[11] M. Li, R. Lang, D. Le Vine and E. Dinnat, “P Band Seawater Dielectric Measurements at Low and High Salinities,” IGARSS2024 – 2024 IGARSS International Geoscience and Remote Sensing Symposium, Athens, Greece, 2024, pp 5839-5842, doi: 1109/IGARSS53475.2024.10641522

[12] R. Lang, M. Li, B. O’Dell, Y. Zhou and D. Le Vine, "Measurement of Dielectric Constant of Seawater at P Band," IGARSS 2023 - 2023 IEEE International Geoscience and Remote Sensing Symposium, Pasadena, CA, USA, 2023, pp. 3988-3990, doi: 10.1109/IGARSS52108.2023.10282525.

[13] L.F. Chen, C. K. Ong, V. V. Varadan, and V. K. Varadan (2004), Microwave Electronics, chap. 6, Wiley, Chichester, England.

[14] TEOS-10: IOC, SCOR and IAPSO, 2010: The international thermodynamic equation of seawater – 2010: Calculation and use of thermodynamic properties. Intergovernmental Oceanographic Commission, Manuals and Guides No. 56, UNESCO (English), pp.196. Available from: https://www.teos-10.org; See Section 2.3 in http://www.teos-10.org/pubs/TEOS-10_Manual.pdf.

[15] T.J. McDougall and P.M. Barker, 2011: Getting started with TEOS-10 and the Gibbs Seawater (GSW) Oceanographic Toolbox, 28pp., SCOR/IAPSO WG127, ISBN 978-0-646-55621-5.

[16] E.L. Lewis, “The practical salinity scale 1978 and its antecedents”, IEEE J. Oceanic Eng., OE-5(1), 3–8, 1980.

[17] R. Somaraju and J. Trumpf, “Frequency, temperature and salinity variation of the permittivity of seawater,” IEEE Trans. Antennas Propag., vol. 54, no. 11, pp. 3441–3448, Nov. 2006.

[18] P. J. W. Debye, Polar Molecules. Dover, IL, USA: Dover, 1929.

[19] H. J. Liebe, G. A. Hufford, and T. Manabe, “A model for the complex permittivity of water at frequencies below 1 THz", Int. J. Infr. Millim. Waves, vol. 12, no. 7, pp. 659-675, 1991.

[20] A. Stogryn, “Equations for calculating the dielectric constant of saline water (Correspondence),” IEEE Trans. Microw. Theory Techn., vol. MTT-19, no. 8, pp. 733–736, Aug. 1971.

[21] P. W. Rosenkranz, “A model for the complex dielectric constant of supercooled liquid water at microwave frequencies,” IEEE Trans. Geosci. Remote Sens., vol. 53, no. 3, pp. 1387–1393, Mar. 2015.

[22] D.M. Le Vine, Y. Zhou and R. H. Lang, "Model for Dielectric Constant of Seawater Based on L-Band Measurements with Conductivity by Definition," IEEE Geoscience and Remote Sensing Letters, vol. 19, pp. 1-5, 2022, Art no. 1506605, doi: 10.1109/LGRS.2022.3221888.

[23] E. Dinnat, D. Le Vine, J. Boutin, T. Meissner, and G. Lagerloef, “Remote sensing of sea surface salinity: Comparison of satellite and in situ observations and impact of retrieval parameters,” Remote Sens., vol. 11, no. 7, p. 750, Mar. 2019.

[24] N. Reul et al., “Sea surface salinity estimates from spaceborne L-band radiometers: An overview of the first decade of observation (2010–2019),” Remote Sens. Environ., vol. 242, Jun. 2020, Art. no. 111769, doi: 10.1016/j.rse.2020.111769.

[25] T. Meissner, F. J. Wentz, and Le Vine, “The salinity retrieval algorithms for the NASA aquarius version 5 and SMAP version 3 releases,” Remote Sens., vol. 10, p. 1121, Jul. 2018, doi: 10.3390/rs10071121.

[26] J. T. Johnson et al., "Microwave Radiometry at Frequencies From 500 to 1400 MHz: An Emerging Technology for Earth Observations," in IEEE Journal of Selected Topics in Applied Earth Observations and Remote Sensing, vol. 14, pp. 4894-4914, 2021, doi: 10.1109/JSTARS.2021.3073286.

[27] G. Macelloni et al., "Cryorad: A Low Frequency Wideband Radiometer Mission for the Study of the Cryosphere," IGARSS 2018 - 2018 IEEE International Geoscience and Remote Sensing Symposium, Valencia, Spain, 2018, pp. 1998-2000, doi: 10.1109/IGARSS.2018.8519172.